









Spectroscopic quantification of photophysical constants in Sn-Pb perovskites

Joudi Alahmadi
jodijodi2018@gmail.com

Mentor: Samuel Stranks
sds65@cam.ac.uk

Mentor: Robert Westbrook
rw794@cam.ac.uk

August 27, 2025

Abstract

Tin–lead (Sn–Pb) halide perovskites are attractive candidates for narrow-bandgap absorbers in tandem solar cells. However, their performance is constrained by elevated hole background densities in addition to nonradiative recombination. In the present study, we combine steady-state photoluminescence quantum yield (PLQY) and time-resolved photoluminescence (TRPL) measurements to extract key photophysical parameters, such as the background hole density (p_0) and the recombination rate constants. Films that are not treated exhibit high p_0 values that agree with self-doping from Sn vacancy formation, and they have short PL lifetimes of less than 15 ns. Compared to other post-treatments, self-doping is most effectively suppressed by post-treatment, leading to a reduction in p_0 values by more than an order of magnitude. Furthermore, additional passivation with ethylenediammonium diiodide ($EDAI_2$) reduces p_0 values to some of the lowest reported for Sn–Pb perovskites. Significantly, we also identify a correlation between p_0 and the monomolecular recombination constant (a), which shows that increased background doping enhances nonradiative pathways. Therefore, this method of analysis demonstrates the relationship between doping, trapping, and passivation, and highlights that specific chemical treatments are effective in reducing self-doping pathways.

Contents

Abstract **1**

1 Introduction **3**

2 Modeling the Effect of a and p_0 on the Shape of the PLQY **3**

3 Extracting p_0, a, and b Workflow **5**
3.1 Bowman Method 5
3.2 Westbrook Method 6
3.3 Application to Different Samples 8

4 Analyzing the Data **8**
4.1 Correlation Between a and p_0 9

5 Conclusion and Future Work **11**

6 Appendix **13**

1 Introduction

In the accelerated race to pursue more sustainable energy technologies, halide perovskites have emerged as a good semiconductor absorber for next-generation solar cells, due to their high Power conversion efficiency (PCE) achieved via lower cost and solution-based process [1]. The chemical formula of perovskite is ABX_3, where A refers to a monovalent cation (e.g., MA^+, FA^+, Cs^+), B to a divalent metal cation (e.g., Pb or Sn), and X to a halide anion [2].

The substitution of tin in perovskite designs is another way to reduce ecological concerns while narrowing the bandgap to approximately 1.3 eV with high values of absorption coefficient ($> 10^5\,\mathrm{cm}^{-1}$) and high carrier mobilities, making them excellent candidates in all-perovskite tandem solar architectures. However, they often suffer from instability and defect formation due to the oxidation process of Sn from Sn^{2+} to Sn^{4+} [3]. Oxidation processes decrease the stability of the device because it increases the background hole density due to self-doping, and also enhance nonradiative recombination, prompting defect-management strategies such as additives (SnF_2, metallic Sn) and compositional engineering (FA^+/Cs^+) to suppress oxidation and improve PCE and stability [4].

Optical spectroscopy techniques such as steady-state photoluminescence, time-resolved photoluminescence, and photoluminescence quantum yield can provide quantitative insight into recombination mechanisms, constants, nonradiative losses, and background hole density [5][6]. Such techniques have been widely applied to lead-halide perovskites. However, analogous conduct in tin-containing systems—especially those that map spatial heterogeneity, self-doping, and microstructure with carrier lifetime—remains limited [7]. Notably, recent work by Westbrook et al. (2024) showed that local variations in the equilibrium hole density, p_0, strongly drive nonradiative recombination losses in tin halide perovskites, underscoring the importance of quantifying and mapping p_0 in these materials [8]. However, most reports provide ensemble data that average over large areas, obscuring microscale variations in p_0 and recombination rates that can be performance-limiting.

This project fills the void by systematically studying the photophysical properties of mixed Sn–Pb based perovskite films produced under different dopant and processing conditions. By extracting the key parameters—equilibrium carrier density (p_0), monomolecular recombination constant (a), and bimolecular recombination constant (b)—and correlating them with spatially resolved PL mapping, we build detailed insights into how processing and microstructure influence stability, self-doping, and nonradiative recombination, thereby serving as guidelines toward stable, high-efficiency tin perovskite solar cells.

2 Modeling the Effect of a and p_0 on the Shape of the PLQY

The photoluminescence quantum yield (PLQY) in a doped semiconductor can be described as

$$\mathrm{PLQY} = \frac{bp_0 n + bn^2}{bp_0 n + an + cp_0^2 n + bn^2 + cn^3}, \tag{1}$$

where n is the excess carrier density, a is the monomolecular (Shockley–Read–Hall) nonradiative recombination rate constant, b is the bimolecular radiative constant, c is the Auger constant for doped semiconductors, and p_0 is the equilibrium hole density due to doping. In the radiative term, n is replaced by $n + p_0$.

In doped semiconductors, p_0 is significant. Thus, the expression simplifies to

$$\mathrm{PLQY} = \frac{bp_0}{bp_0 + a + cp_0^2} = \frac{bp_0}{bp_0 + a}, \tag{2}$$

where a represents the effective nonradiative recombination contribution.

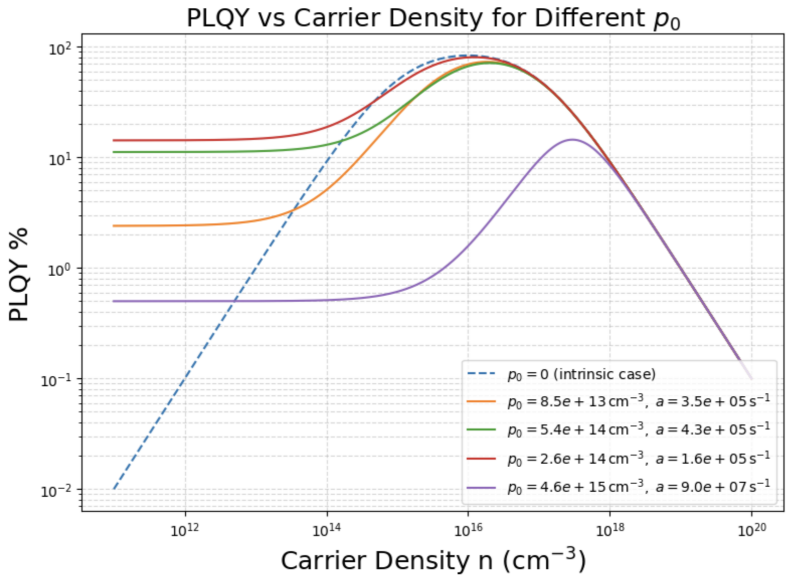


Figure 1: Modeled PLQY versus carrier density for different p_0 values and fixed parameters $n = 10^{11}$–$10^{20}\,\mathrm{cm}^{-3}$, $b = 1 \times 10^{-10}\,\mathrm{cm}^3\,\mathrm{s}^{-1}$, and $c = 1 \times 10^{-27}\,\mathrm{cm}^6\,\mathrm{s}^{-1}$.

For low p_0 values, PLQY curves rise with excitation due to trap filling, whereas TRPL lifetimes first increase and then decrease. When p_0 increases, the recombination begins to favor bimolecular radiative processes at low injection, with PLQY remaining on a plateau and TRPL decays turning into a mono-exponential of the form $n < p_0$. However, very high p_0 causes Auger losses, thereby reducing both PLQY and lifetime for all excitation densities [5].

Figure 1 illustrates this behavior: at low p_0 ($10^{15}\,\mathrm{cm}^{-3}$), PLQY rises sharply with increasing n due to trap filling under SRH recombination, and then shows a broad maximum before Auger recombination dominates at $n \gtrsim 10^{18}\,\mathrm{cm}^{-3}$. At moderate p_0, radiative recombination with dopant holes dominates for $n < p_0$, resulting in a broad PLQY plateau.

3 Extracting p_0, a, and b Workflow

To obtain a complete consistent set of photophysical constants, an analysis workflow has been developed that combines elements from two complementary approaches: the method of Bowman et al.[9] and that of Westbrook et al. [8].

3.1 Bowman Method

First, the method described by Bowman et al. was followed, where p_0 was derived from time-resolved photoluminescence (TRPL) data collected by an ICCD camera. For each excitation fluence, $PL(t)$, or the initial PL intensity right after the excitation pulse, was obtained from the decay trace. From the absorbed photon flux, the corresponding initial carrier density, n_0, was then calculated.

Under the low-injection rate equation:

$$PL(t) = bp_0n_0 + bn_0^2, \tag{3}$$

Dividing by n_0:

$$\frac{PL(t)}{n_0} = M + Nn_0, \tag{4}$$

where $M = bp_0$ and $N = b$. By fitting $PL(t)/n_0$ versus n_0 with a linear function, M and N are extracted directly. The background hole density is then obtained from:

$$p_0 = \frac{M}{N}. \tag{5}$$

As shown in Figure 2, $M = 1.92 \times 10^{-15}$ and $N = 3.56 \times 10^{-30}$, from which:

$$p_0 = \frac{M}{N} = 5.39 \times 10^{14}\,\mathrm{cm}^{-3}. \tag{6}$$

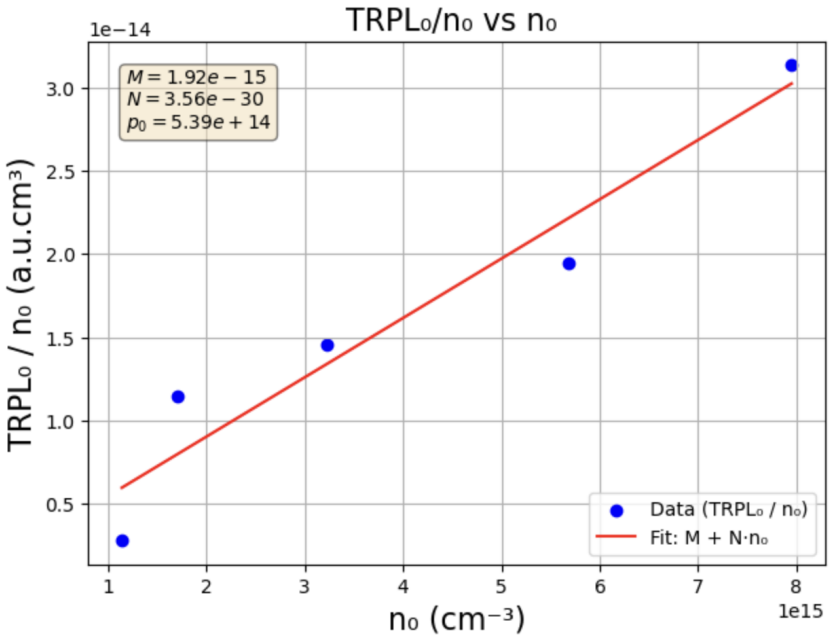


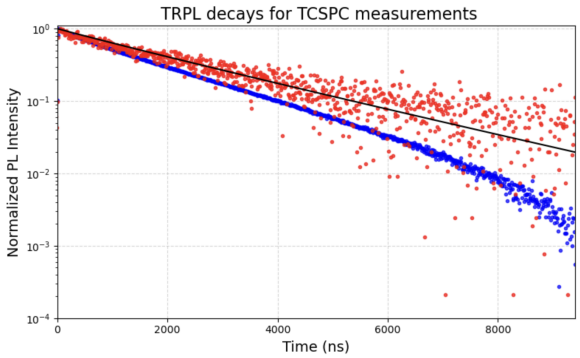
Figure 2: Determination of p_0 using the Bowman *et al.* method. Plot of TRPL_0/n_0 versus n_0 obtained from fluence-dependent ICCD TRPL measurements. The solid red line is a linear fit to $\mathrm{TRPL}_0/n_0 = M + Nn_0$, yielding $M = 1.92 \times 10^{-15}$ and $N = 3.56 \times 10^{-30}$. From $p_0 = M/N$, the background hole density is determined to be $5.39 \times 10^{14}\,\mathrm{cm}^{-3}$.

3.2 Westbrook Method

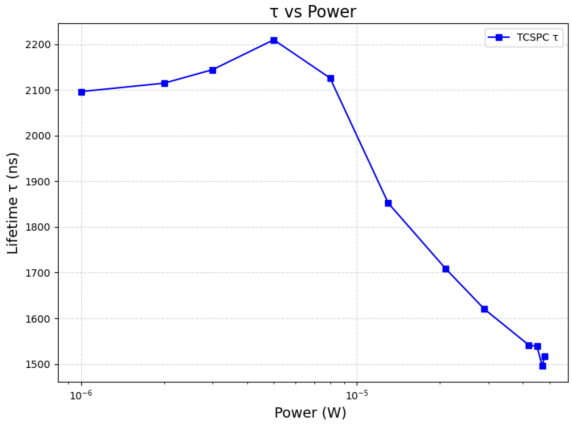
On the other side, Westbrook et al. combined low-injection steady-state PLQY measurements with time-correlated single-photon counting (TCSPC) TRPL measurements to extract p_0, a, and b.

At first, fluence-dependent TRPL experiments were carried out using a spectrofluorometer in Multi-Channel Scaling (MCS) mode. Representative TRPL decay curves for different excitation powers are shown in Figure 3a, with extracted lifetimes plotted against excitation power in Figure 3b. Excitation fluence was decreased until the obtained mono-exponential lifetime τ remained constant and the log-scale of the decay was linear, as shown in the fitted curve in Figure 3a.Which first order kinetics signify that $an + bnp_0$ dominates (could be trapping or doping or both) rather than the photogenerated carrier density.

Then, steady-state PLQY was measured for the same sample. The dependence of PLQY on excitation power is plotted in Figure 4 where a low-fluence plateau is observed, corresponding to the same carrier density regime in which τ was determined.



(a) Decay curve for 45% excitation power. Stretched exponential fit yields $\tau = 2.037\,\mu$s, $\beta = 0.93$.



(b) Extracted τ as a function of excitation power.

Figure 3: (a) TRPL decay and stretched exponential fitting at 45% excitation power. (b) Extracted lifetimes versus carrier density.

In the low-injection limit, it can be said:

$$\mathrm{PLQY} = \frac{bp_0}{a + bp_0}, \qquad \frac{1}{\tau_{\mathrm{eff}}} = a + bp_0. \tag{7}$$

From these, we conclude:

$$p_0 = \frac{\mathrm{PLQY}}{b\tau_{\mathrm{eff}}}, \qquad a = \frac{1}{\tau_{\mathrm{eff}}} - bp_0, \qquad b = \frac{\mathrm{PLQY}}{\tau_{\mathrm{avg}}\, p_0}. \tag{8}$$

Steady-state PLQY was measured over a wide range of excitation powers using an integrating sphere, with results shown in Figure 4. The data are plotted on a log–log scale to clearly capture variations across several orders of magnitude in excitation power. At low excitation, the PLQY shows a more or less flat region at approximately 11%, indicative of a recombination mechanism dominated by doping-limited bimolecular radiative processes ($\Delta n \ll p_0$). This plateau value was used in the analysis with the Westbrook method to remain consistent with the low-injection lifetimes from TCSPC measurements.

It is important to emphasize that this 11% PLQY value holds in the range of very low injection. Subsequently, as the excitation is made stronger, trap sites get filled, therefore the PLQY rises to a maximum and then decreases, a behavior attributed to the onset of nonradiative losses and higher-order recombination processes.
By using the value of τ_{avg}, PLQY, and p_0 extracted from the Bowman method, we can calculate b from the relation:

$$b \approx 1 \times 10^{-10}\,\mathrm{s}^{-1}. \tag{9}$$

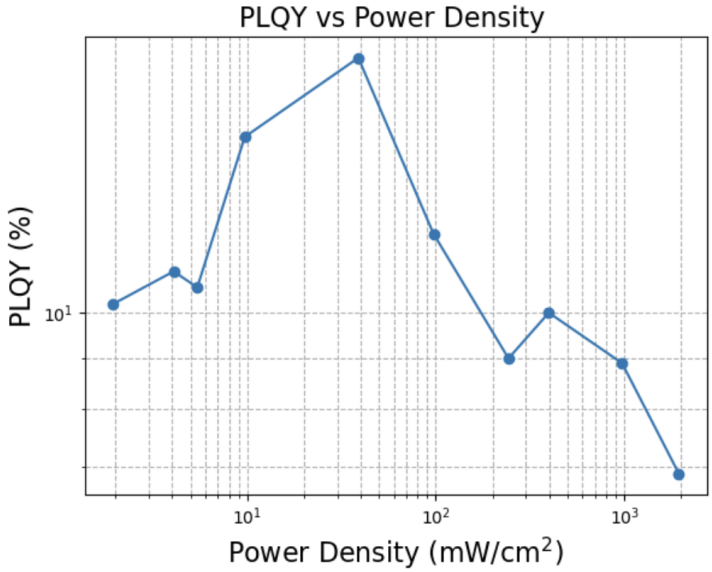


Figure 4: Steady-state PLQY as a function of excitation power plotted on a log–log scale. At low excitation power, the PLQY exhibits a plateau value of approximately 11%.

By combining the low-injection PLQY of 11% as shown in Figure 4 with the corresponding TCSPC lifetime of 2 μs, and using b obtained from both Bowman and Westbrook methods, we calculated:

$$p_0 = 5.4 \times 10^{14}\,\mathrm{cm}^{-3}, \qquad a = 4.3 \times 10^{5}\,\mathrm{s}^{-1}. \tag{10}$$

3.3 Application to Different Samples

The workflow described above was first illustrated using data from the "treated, non-passivated" sample. The same combined Bowman–Westbrook analysis was then applied to three additional samples: a "treated and passivated" film, an "treated, non-passivated" film, and an "untreated, non-passivated" film. This allowed a direct comparison of p_0 and a across different processing conditions, and specifically to assess how $EDAI_2$ passivation affects these photophysical constants (measurements details can be found in appendix).

4 Analyzing the Data

To place our extracted p_0 values in context, literature data for background hole densities in Sn–Pb perovskites were compiled. These values were obtained using various electrical and optical techniques, as summarized in Table 1. We then added the values obtained in this work for the four Sn–Pb perovskite films that have been analyzed: untreated/non-passivated, treated/non-passivated (1), treated/non-passivated (2), and

treated/passivated, determined via the combined Bowman–Westbrook analysis.

This side-by-side comparison allows for a direct assessment of how our samples perform and highlights the impact of processing treatment and $EDAI_2$ passivation on p_0.

tabularx

Table 1: Background hole densities (p_0) in Sn–Pb perovskites from literature and this work.

Composition / Sample	p_0 **(cm^{-3})**	**Reference**	**Technique**
$FA_{0.6}MA_{0.4}Sn_{0.6}Pb_{0.4}I_3$	7.20×10^{15}	Tong *et al.*, *Nat. Energy*, 2022	Hall Effect
$FA_{0.6}MA_{0.4}Sn_{0.6}Pb_{0.4}I_3$	1.30×10^{14}	Tong *et al.*, *Nat. Energy*, 2022	Hall Effect
$CH_3NH_3Sn_{0.5}Pb_xI_3$	1.00×10^{14}	Stoumpos *et al.*, *Inorg. Chem.*, 2013	Hall Effect
$FA_{0.7}MA_{0.3}Sn_{0.5}Pb_{0.5}I_3$	6.00×10^{14}	Thiesbrummel *et al.*, *Adv. Energy Mater.*, 2021	Two-point probe
FA $Pb_{0.5}Sn_{0.5}I_3$	2.50×10^{14}	Bowman *et al.*, *ACS Energy Lett.*, 2019	Optical (PLQY)
FA $Pb_{0.5}Sn_{0.5}I_3$	1.00×10^{15}	Bowman *et al.*, *ACS Energy Lett.*, 2019	Optical (PLQY)
$FA_{0.5}MA_{0.45}Cs_{0.05}Pb_{0.5}Sn_{0.5}I_3$	1.00×10^{16}	Yang *et al.*, *Nat. Commun.*, 2019	Capacitance–voltage
$FA_{0.5}MA_{0.45}Cs_{0.05}Pb_{0.5}Sn_{0.5}I_3$	4.20×10^{15}	Yang *et al.*, *Nat. Commun.*, 2019	Capacitance–voltage
untreated, non-passivated sample	$\mathbf{4.55 \times 10^{15}}$	*This work*	Optical (PLQY–TRPL)
treated, non-passivated sample (1)	$\mathbf{5.40 \times 10^{14}}$	*This work*	Optical (PLQY–TRPL)
treated, non-passivated sample (2)	$\mathbf{2.57 \times 10^{14}}$	*This work*	Optical (PLQY–TRPL)
treated, passivated sample	$\mathbf{8.52 \times 10^{13}}$	*This work*	Optical (PLQY–TRPL)

The literature values for p_0 in Sn–Pb perovskites span over two orders of magnitude: from $\sim 10^{14}\,\mathrm{cm}^{-3}$ in high-quality films measured by Hall effect or optical methods to $\sim 10^{16}\,\mathrm{cm}^{-3}$ in heavily doped materials. Differences in reported values stem from variations in composition, fabrication conditions, and measurement technique.

The values obtained in this work show a clear trend with processing condition. The untreated, non-passivated sample exhibited a background hole density in the higher range of literature values, indicating a relatively high level of self-doping and a significant concentration of acceptor defects. After treatment without passivation, the first sample showed some improvement over the untreated film but still remained higher than other treated cases. A second treated, non-passivated sample reached p_0 values comparable to the lowest ever reported for well-processed Sn–Pb perovskites, demonstrating that the treatment can efficiently suppress self-doping and may lower defect density. Finally, the treated and passivated sample achieved the lowest p_0 overall, falling below most values reported in the literature, confirming that $EDAI_2$ passivation further reduces the background hole density beyond the effect of treatment alone.

Overall, the comparison highlights that the combination of processing treatment and $EDAI_2$ passivation produces films with exceptionally low background doping, a key requirement for achieving high open-circuit voltage and long carrier lifetimes in Sn–Pb perovskite devices.

4.1 Correlation Between a and p_0

Plotting a versus p_0, as shown in Figure 5, reveals a general positive correlation between the background hole density and the monomolecular nonradiative recombination rate con-

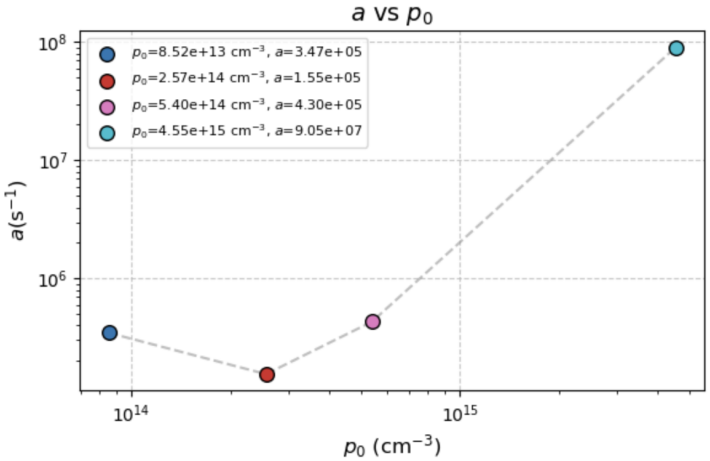


Figure 5: Determination of p_0 using the Bowman *et al.* method. Plot of TRPL_0/n_0 versus n_0 obtained from fluence-dependent ICCD TRPL measurements. The solid red line is a linear fit to $\mathrm{TRPL}_0/n_0 = M + Nn_0$, yielding $M = 1.92 \times 10^{-15}$ and $N = 3.56 \times 10^{-30}$. From $p_0 = M/N$, the background hole density is determined to be $5.39 \times 10^{14}\,\mathrm{cm}^{-3}$.

stant. Samples with higher p_0 tend to exhibit larger a values, indicating that self-doping is linked to an increased density of defect states that promote trap-assisted recombination.

The untreated–unpassivated sample ($p_0 = 4.55 \times 10^{15}\,\mathrm{cm}^{-3}$) shows the highest a ($9.05 \times 10^7\,\mathrm{s}^{-1}$), consistent with severe self-doping and high defect density. The treated–unpassivated samples (Samples 4 and 6) occupy intermediate positions, with lower p_0 and correspondingly smaller a, suggesting that processing treatment reduces both self-doping and trap-mediated recombination.

Interestingly, the treated–passivated sample has the lowest p_0 but not the lowest a. This unexpected result could be due to a different trap distribution or the possibility that passivation targets primarily surface states, leaving some bulk nonradiative channels unaffected. This highlights the complexity of correlating background doping with recombination dynamics, and suggests that a full understanding requires both spatially resolved mapping and complementary spectroscopic techniques.

5 Conclusion and Future Work

With combined PLQY and TRPL measurements, we determined the same photophysical parameters—p_0, a, and b—for the untreated, treated, and passivated Sn–Pb perovskite films. A key takeaway is that chemical treatment suppresses self-doping, effectively decreasing p_0 by more than an order of magnitude. Additional passivation with ethylenediammonium diiodide ($EDAI_2$) yields the lowest background hole densities reported for this material system. These reductions in p_0 coincide with higher PLQY values and longer carrier lifetimes, indicating a sharp decrease in nonradiative recombination.

While these results show clear trends, there are limitations to this analysis. Although passivation with $EDAI_2$ was observed to reduce p_0, the extracted a value did not improve compared to the treated–unpassivated sample.the hypothesis become that the underlying reason may relate to differences in defect distributions or measurement uncertainties. Specifically, $EDAI_2$ may repair or fill shallow traps or Sn vacancies but does not significantly affect deep traps [10], meaning that a remains almost the same in both passivated and unpassivated samples. Another avenue for improvement would be to calculate carrier densities corresponding to the excitation powers used in each instrument (fluorimeter and PLQY), as these were not determined directly, preventing full cross-calibration of datasets. Finally, applying the PLQY+TRPL workflow to microscale PL mapping could enable extraction of spatial maps of p_0, a, and b, thereby providing detailed insight into how local heterogeneity influences the overall photophysical behavior of the films, since perovskite materials are well known for their structural and electronic heterogeneity.

References

[1] JH Im et al. "Growth of $CH_3NH_3PbI_3$ cuboids with controlled size for high-efficiency perovskite solar cells". In: *Nature Nanotechnology* 9.11 (2014), pp. 927–932.

[2] M Mohan, NP Shetti, and TM Aminabhavi. "Perovskites: A new generation electrode materials for storage applications". In: *Journal of Power Sources* 574 (2023), p. 233166.

[3] C Cho et al. "Efficient vertical charge transport in polycrystalline halide perovskites revealed by four-dimensional tracking of charge carriers". In: *Nature Materials* 21.12 (2022), pp. 1388–1395.

[4] G Min et al. "The Effect of Antisolvent Treatment on the Growth of 2D/3D Tin Perovskite Films for Solar Cells". In: *ACS Energy Letters* 10.1 (2025), pp. 254–262.

[5] A Treglia et al. "Effect of electronic doping and traps on carrier dynamics in tin halide perovskites". In: *Materials Horizons* 9.6 (2022), pp. 1763–1773.

[6] S Srivastava et al. "Advanced spectroscopic techniques for characterizing defects in perovskite solar cells". In: *Communications Materials* 4.52 (2023).

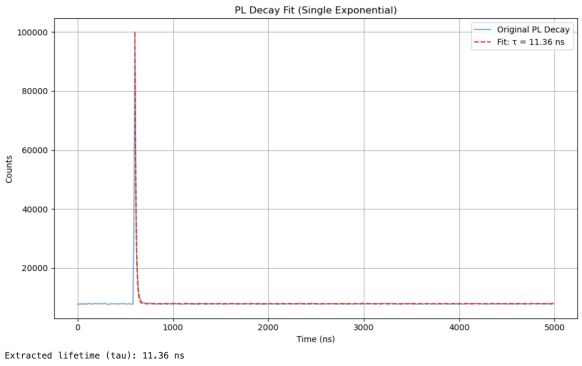
[7] E Aktas et al. "Challenges and strategies toward long-term stability of lead-free tin-based perovskite solar cells". In: *Communications Materials* 3.104 (2022).

[8] RJE Westbrook et al. "Local Background Hole Density Drives Nonradiative Recombination in Tin Halide Perovskites". In: *ACS Energy Letters* 9.2 (2024), pp. 732–739.

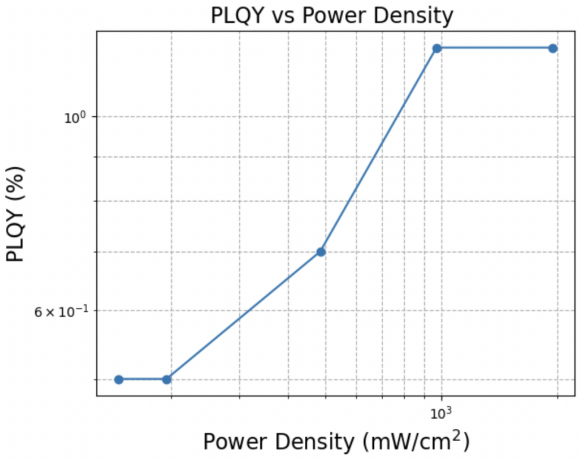
[9] AR Bowman et al. "Extracting Decay-Rate Ratios From Photoluminescence Quantum Efficiency Measurements in Optoelectronic Semiconductors". In: *Physical Review Applied* 17.4 (2022), p. 044026.

[10] FJ Berger et al. "How Halide Alloying Influences the Optoelectronic Quality in Tin-Halide Perovskite Solar Absorbers". In: *ACS Energy Letters* 8.9 (2023), pp. 3876–3882.

6 Appendix

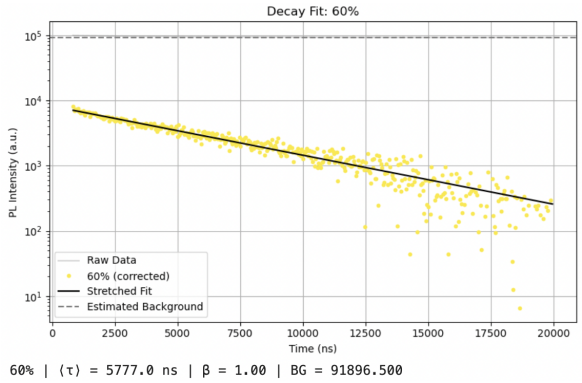


(a) TRPL decay of the non-passivated, untreated sample at 70% intensity. Fitted with a single exponential (red dashed line), yielding a lifetime of 11.36 ns.

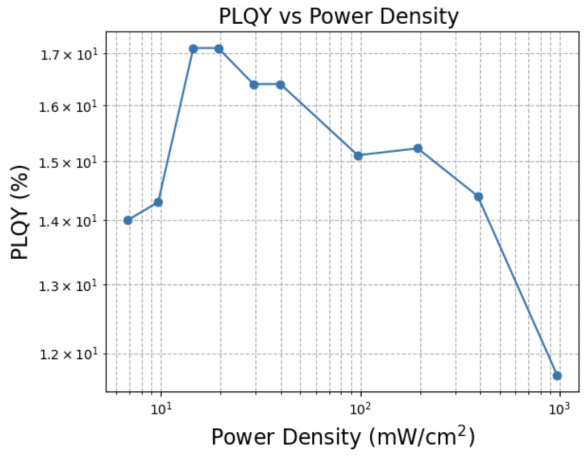


(b) Steady-state PLQY versus excitation power for the non-passivated, untreated sample, plotted on a log–log scale. The PLQY remains below 0.5% across all measured excitation powers.

Figure 6: TRPL and steady-state PLQY for the untreated, non-passivated sample. (a) Time-resolved photoluminescence decay with exponential fitting. (b) PLQY as a function of excitation power.

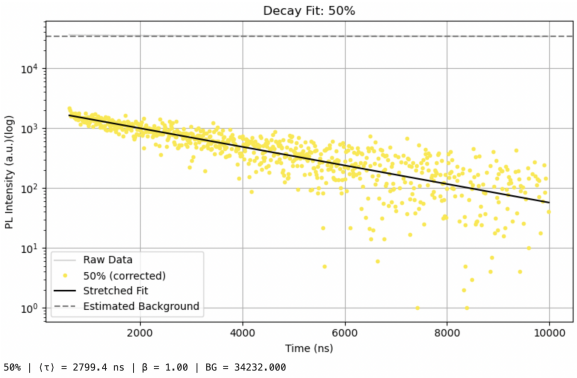


(a) Time-resolved photoluminescence (TRPL) decay of the treated, non-passivated sample, measured at 60% intensity using TCSPC. Fitted with a stretched exponential (black line), yielding a low-injection lifetime of $\tau = 5\,\text{ns}$.

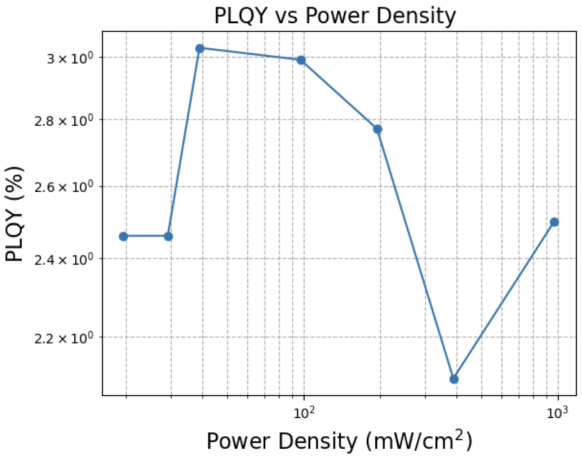


(b) Steady-state PLQY of the treated, non-passivated sample as a function of excitation power, plotted on a log–log scale. At low excitation power, the PLQY shows a plateau at $\sim 13\%$.

Figure 7: TRPL and steady-state PLQY for the treated, non-passivated sample. (a) TRPL decay and stretched exponential fitting. (b) Steady-state PLQY versus excitation power.



(a) Time-resolved photoluminescence (TRPL) decay of the treated, passivated sample at 50% intensity using TCSPC. Fitted with a stretched exponential (black line), yielding a low-injection lifetime of $\tau = 2\,\text{ns}$.



(b) Steady-state PLQY of the treated, passivated sample as a function of excitation power, plotted on a log–log scale. At low excitation power, the PLQY shows a plateau at $\sim 2\%$.

Figure 8: TRPL and steady-state PLQY for the treated, passivated sample. (a) TRPL decay with stretched exponential fitting. (b) Steady-state PLQY versus excitation power.

Resources and Tools Used

Spectroscopic Equipment

- Fluorimeter for steady-state photoluminescence (PL) and Multi-Channel Scaling (MCS) mode for time-resolved photoluminescence (TRPL) measurements.
- Intensified CCD (ICCD) camera and time-correlated single-photon counting (TCSPC) setup for TRPL measurements.
- Photoluminescence quantum yield (PLQY) measurements performed using a fluorimeter equipped with an integrating sphere.

Data Analysis Software

- Python (`NumPy`, `SciPy`, `Matplotlib`, `Pandas`) for modeling, curve fitting, and data visualization.

Collaboration and Mentoring

- Support from mentors and group members in the Stranks Laboratory (University of Cambridge) regarding measurements and their interpretation.